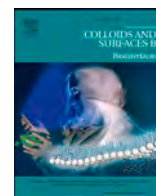




Contents lists available at ScienceDirect

Colloids and Surfaces B: Biointerfaces

journal homepage: www.elsevier.com/locate/colsurfb

Electrospun nanoyarn and exosomes of adipose-derived stem cells for urethral regeneration: Evaluations in vitro and in vivo

Liyang Wang^{a,1}, Wei Cheng^{c,1}, Jingjing Zhu^{d,1}, Wenyao Li^{a,*}, Danyang Li^a, Xi Yang^f, Weixin Zhao^g, Mingjun Ren^h, Jieji Ren^h, Xiumei Mo^d, Qiang Fu^{b,e}, Kaile Zhang^{b,e,**}

^a School of Materials Engineering, Shanghai University of Engineering Science, Shanghai 201620, China

^b The Department of Urology, Affiliated Sixth People's Hospital, Shanghai Jiao Tong University, Shanghai 200233, China

^c School of Public Health, Shanghai Jiao Tong University School of Medicine, Shanghai 200025, China

^d State Key Lab for Modification of Chemical Fibers & Polymer Materials, College of Chemistry & Chemical Engineering and Biotechnology, Donghua University, Shanghai 201620, China

^e Shanghai Eastern Institute of Urologic Reconstruction, Shanghai 200233, China

^f Novaprint Therapeutics Suzhou Co., Ltd, Suzhou 215000, China

^g Wake Forest Institute for Regenerative Medicine, Winston-Salem, NC, United States

^h State Key Laboratory of Mechanical System and Vibration, School of Mechanical Engineering, Shanghai Jiao Tong University, Shanghai 200233, China

ARTICLE INFO

Keywords:

Electrospinning

Nanoyarn

Adipose-derived stem cells

Exosomes

ABSTRACT

Regeneration of urethral defects has been difficult in the clinic. To address it, the collagen/ poly (L-lactide-caprolactone) (P(LLA-CL)) nanoyarn scaffold delivering adipose-derived stem cells' exosomes (ADSC-exos) was fabricated. The multipotential differentiation potential of ADSCs were confirmed by Adipogenic, osteogenic, and chondrogenic differentiation. The 3-(4,5-dimethylthiazol-2-yl)–2,5-diphenyltetrazolium bromide assay shows that 50% concentration of ADSC-exos nanoyarn scaffold dramatically enhanced the cell viability of fibroblasts. The ADSC-exos nanoyarn scaffold for human foreskin fibroblasts (HFFs) and human urethral scar fibroblasts (HSFs) shows good biocompatibility: the production of inflammatory factors IL-6 and Col 1A1 was less, indicating that ADSC-exos had the minimal inflammatory effect of cells. Besides, the cells on the ADSC-exos nanoyarn scaffold did not appear to contribute to DNA damage in the same way as the normal cell's growth did. The HFFs seeding on the ADSC-exos nanoyarn scaffold shows a typical morphology of extending outwards. Urethral repair with ADSC-exos nanoyarn scaffold did not lead to either a sign of urethral stricture or scar formation after 4 weeks post-surgery. The deposition of collagen was less and the epithelial cells formed multiple layer epithelium. The treatment of ADSC-exos stimulated epithelization and vascularization. And the transition from an inflammatory state to a regenerative state was promoted. The ADSC-exos-treated group did not promote the over-proliferation of fibroblasts and the expression of Collagen I. Therefore, the ADSC-exos nanoyarn scaffold has evident, positive effects on wound healing and tissue fibrosis inhibition.

1. Introduction

Hypospadias and urethral stricture are common urological defects, which remain to be difficult problems in urology as they seriously affect the voiding function and life quality for patients. Reconstruction of the urethral defects is usually done through transplanting autologous tissues, but with a serious injury to the harvesting location [1–3]. Since unsatisfactory clinical outcomes and frequent complications are

introduced by current clinical treatments, bioengineered tissue has become the most hopeful treatment option for urethral repair [2]. Briefly, there are three basic elements in tissue engineering: cell, scaffold, and bioactive factors [4,5]. The poor result of tissue-engineered urethra might come from the deficient neovascularization and the diminished levels of proangiogenic factors production [6–8]. So, there is an urgent need for the functional urethra to be properly reconstructed by novel biomaterials in order to simultaneously promote wound

* Corresponding author.

** Corresponding author at: The Department of Urology, Affiliated Sixth People's Hospital, Shanghai Jiao Tong University, Shanghai 200233, China.

E-mail addresses: liwenyao@sues.edu.cn (W. Li), jamesqfu@aliyun.com (Q. Fu), great_z0313@126.com (K. Zhang).

¹ Equal contributors

<https://doi.org/10.1016/j.colsurfb.2021.112218>

Received 22 September 2021; Received in revised form 2 November 2021; Accepted 12 November 2021

Available online 15 November 2021

0927-7765/© 2021 Elsevier B.V. All rights reserved.

healing and prevent fibrosis or scar formation.

Regarding biomaterials and fabrication technology of scaffolds, electrospinning is a classic method of generating fibers with a range of micrometers to nanometers. Interestingly, conjugated electrospinning has been used to fabricate nanoyarn scaffolds to improve the issue of densely packed fibers [9,10]. Co-axial electrospinning is also widely used to deliver bioactive factors. During the fibrillogenesis of collagen, collagen nanofibers become similar to the extracellular matrix (ECM) structure and may induce tissue alignment with anisotropic strain [11]. Collagen, as the main component of the extracellular matrix protein, possesses natural biocompatibility for urothelial cells to expand and differentiate [12,13]. However, the pure collagen scaffold lacking in mechanical support properties is fragile. Therefore, the poly (L-lactide-co-caprolactone) (P(LLA-CL)) with good biocompatibility and biological degradability, especially with good mechanical properties, was blended to collagen. Previous studies have shown that the nanoyarn scaffold can be significantly improved in pore size and porosity and can promote fibroblasts attachment, proliferation and spreading [14,15]. The nanoyarn scaffold delivering the drug thus presents a desirable treatment for urethral tissue reconstruction.

Adipose-derived mesenchymal stem cells (ADSCs), one type of multipotent stem cells, have the ability of self-renewal and multidirectional differentiation. The regenerative capacity of tissues was significantly promoted by encouraging the formation of new blood vessels and regulating inflammation [10,16]. Some studies have found that ADSCs can secrete biologically active factors (including growth factors, cytokines, and exosomes, etc.), which promote cell proliferation, differentiation, and migration [17–21]. Exosomes, a diameter of 30–150 nm, are small membrane vesicles of endocytic origin [22–26]. Exosomes include proteins, mRNA, and microRNA, which can bring complex biological information and release it into target cells [25–27]. In addition, exosomes are a paracrine mediator and may exist between MSCs and target cells [25,28,29]. Simona et al. have demonstrated the beneficial influence of biochemical signaling and stimuli from MSCs in tissue regeneration and vascularization in an interconnected co-culture system. Many studies suggest the important roles of ADSCs exosomes (ADSC-exos), e.g., migration and proliferation of cell and collagen synthesis. Therefore, in this study, we hypothesize that the nanoyarn scaffold delivering ADSC-exos has an affirmative influence on the promotion of urethral repair, wound healing, or the reconstruction of functional urethra.

2. Materials and methods

2.1. Materials

Collagen I was obtained from Sichuan Ming-Rang Bio-Tech Co., Ltd. (Chengdu, China). P(LLA-CL) was purchased from Jinan Daigang bioengineering Co. Ltd. (Jinan, China) and the content ratio of L-lactic acid/ ϵ -caprolactone was 50:50, molecular weight about 300,000. ADSC-exos were extracted by high-speed centrifugation. The New Zealand rabbits were purchased by Shanghai sixth people's hospital. All other commercial chemicals were without further purification. All the animal experiments were certified by the ethics committee of the hospital.

2.2. Isolation and culture of ADSCs

New Zealand white rabbit's inguinal fat was collected, 2 cubic centimeters of adipose tissue were cut, and the fat was digested with type 1 collagenase and 0.05% pancreatin / ethylenediaminetetraacetic acid (EDTA) mixture to obtain adipose stem cell suspension. Cells were incubated with low-glucose Dulbecco's modified Eagle's medium (DMEM) (Gibco, USA) supplemented with 10% fetal bovine serum (FBS) and 1% penicillin-streptomycin; after 85–90% confluence, the passage 3–5 cells were used for subsequent experiments of exosomes extraction.

2.3. Multipotential differentiation of ADSCs

The multipotential differentiation potential of ADSCs was evaluated using Adipogenic, Osteogenic, and chondrogenic differentiation assays. For the differentiation studies, ADSCs of passage 5 at a density of 3×10^5 cells/well were seeded in 6-well plates. Adipogenic differentiation, Osteogenic differentiation, and chondrogenic differentiation of ADSCs were performed according to reported procedures with minor modifications [30–32]. After 3 days, the growth medium was replaced with adipogenic medium and osteogenic medium for 14 days, respectively. Then, Oil red O (Sigma, USA) and alizarin red S (Sigma, USA) were used to confirm Adipogenic and Osteogenic differentiation, respectively. The medium was changed twice a week. The chondrogenic differentiation of ADSCs (cell density: 6×10^5 cells/ml) was induced by the StemPro® Chondrogenesis Differentiation kit (Invitrogen Life Technologies) for 21 days. Alcian blue staining was used to confirm chondrogenic differentiation.

2.4. Isolation and identification of rabbit ADSC-derived exosomes

After 80% confluence of ADSCs, the medium was aspirated, washed with PBS, and replaced with serum-free medium. Then, the cells were cultured in an incubator (37 °C, 5% CO₂) for an additional 2 days to collect conditioned medium. Cell debris and dead cells were removed by sequential centrifuging at 500 g for 5 min and 3000 g for 15 min, and then passed by a 0.22 μ m filter (Millipore). Then, using 100KDa molecular weight Amicon® Ultra-15 Centrifugal Filter Device (Millipore), supernatants were concentrated. Exosome precipitation solution was incubated at 4 °C for 12 h. Exosome pellets were washed and resuspended in PBS, then the concentration was measured by BCA protein assay kit. Also, the morphology of exosomes was identified by transmission electron microscopy (TEM; Hitachi, Japan). Nanoparticle Tracking Analysis (NTA) measurements were performed by a ZetaVIEW S/N 17–310 (Particle Metrix, Germany). The x-axis showed the distribution of the size (nm) of exosomes and the y-axis showed the concentration of exosomes is analyzed by Zeta View software.

2.5. Real-time polymerase chain reaction

Total RNA was extracted from ADSCs cultured on T175 flasks with Rneasy Mini kit (QIAGEN, USA) and examined for the expression of target proteins according to previously described methods [15]. The gene expression levels of vascular endothelial growth factor A (VEGFA), tissue inhibitors of metalloproteinase 2 (TIMP2), and WNT1 at the mRNA level were evaluated by quantitative real-time PCR.

2.6. Fabrication of scaffolds

The fabrication of collagen and P(LLA-CL) nanoyarn scaffolds was through co-axial and conjugated electrospinning equipment, which has been reported previously [14,15] (Fig. 2a and c). Briefly, the electrospinning equipment included two syringes with metallic needles in each end and they were connected to a positive voltage of 15 KV and a negative voltage of 15 KV, respectively. Dissolving 1 g collagen/P(LLA-CL) in 1 ml 2, 2, 2-trifluoroethanol (Fine chemicals, Shanghai, China) blended with 0%, 25%, 50%, 75% ADSC-exos (v/v) was used as the core layer solution at a rate of 0.2 ml/h. The solution of the shell layer was 1 g Collagen/P(LLA-CL) dissolved in 2, 2, 2-trifluoroethanol and fed at 0.8 ml/h. Taylor cones were formed by the fibers spun from the two needles and twisted into a yarn, then the nanoyarn was wounded at a speed of 100 r/min by a cylinder collector rotating. Nanofiber scaffold, pure nanoyarn scaffold and ADSC-exos nanoyarn scaffold were fabricated by co-axial and conjugated electrospinning. During the process of nanoyarn scaffold fabrication, the room temperature was maintained at 22–25 °C and the relative humidity was maintained at 40–50%.

2.7. Scanning electron microscopy of nanoyarn scaffolds

The morphology of the nanoyarns with or without ADSC-exos and nanofibers was observed by SEM (Hitachi TM-100, Tokyo, Japan). The specimens were prepared into shape of disks (with a diameter of 1.2 cm), first frozen at $-20\text{ }^{\circ}\text{C}$ and $-80\text{ }^{\circ}\text{C}$ for 2 h, respectively, then freeze-dried in a vacuum state for 24 h, and stored in a vacuum container. The porosity and the angle distribution of the specimens were counted from SEM images. 100 fibers were randomly selected from the SEM images to measure the angle distribution relative to the vertical axis using Image J visualization software (National Institutes of Health, Bethesda, MD, USA) ($n = 3$).

2.8. Mechanical Property Evaluation

The mechanical property of the tensile strength of the ADSC-exos nanoyarn scaffold was measured by a tensile tester (H5K-S, Hounsfield, United Kingdom). According to the requirements of the instrument test, the samples as longitudinal strips with a length of 20 mm and a width of 10 mm were prepared. Then, the sample as the clamp to clamp distance was measured, and conducted for tensile strength, Young's modulus, and elongation at break tests at a speed of 5 mm/min until rupture. The stress and strain data were recorded. Three samples were measured in each group, and the average value and standard deviation were calculated.

2.9. Nanoyarn scaffolds pre-treatment before cell seeding

The sterilization of nanoyarn scaffolds was reported previously using ultraviolet for 8 h [14]. Human foreskin fibroblasts (HFFs) (from the national collection of authenticated cell cultures) and human urethral scar fibroblasts (HSFs) are the cell types to be used in the subsequent experiment. HFFs and HSFs were cultured in high-glucose Dulbecco's modified Eagle's medium supplemented with 10% FBS and 1% penicillin-streptomycin (DMEM complete medium) at $37\text{ }^{\circ}\text{C}$ with 5% CO_2 under a humidified atmosphere.

2.10. MTT assay

Human foreskin fibroblasts (HFFs) with a density of 1×10^5 were seeded on the nanoyarn scaffold samples in each well of 24 well-plate. Cell proliferation after seeding for days 1, 3 and 5 was measured by MTT (5 mg/ml in PBS, Sigma-Aldrich, St. Louis, MO, USA) assay. Briefly, the medium was replaced with 100 μl MTT solution and 900 μl high-glucose DMEM complete medium supplemented added to each well at days 1, 3, 5, then incubated for 4 h at $37\text{ }^{\circ}\text{C}$, and the formazan crystals were dissolved with 100 μl DMSO for at least 20 min. The medium was transferred into a 96-well plate (100 μl per well, $n = 5$). The absorbance of cell solution was measured by an enzyme-labeling instrument at 570 nm (Multiskan MK3, Thermo Fisher Scientific, United States), and the average value and standard deviation were calculated.

2.11. FITC-labeled phalloidin staining

Human foreskin fibroblasts with a density of 1×10^5 were seeded on nanoyarn scaffolds and 50% ADSC-exos nanoyarn scaffolds were stained by using Fluorescein Isothiocyanate (FITC)-labeled phalloidin and DAPI. After 3 and 5 days, the specimens of fibroblasts previously seeding on scaffolds were observed and rinsed twice with PBS (3 min per wash), and then the scaffolds were fixed by using 4% paraformaldehyde for 10 min. Afterward, the cells were penetrated with 0.1% Triton X-100 for 10 min at room temperature. 5 μl FITC-labeled phalloidin (Sigma-Aldrich, USA) mixing in 200 μl PBS was used to stain the cytoskeletons, and the nuclei of the myoblasts on the scaffolds were stained by DAPI (Sigma-Aldrich, USA).

2.12. Biocompatibility and cytotoxicity test

Enzyme-linked immunosorbent assay (ELISA, Enzyme-linked immunosorbent assay, Elabscience, Wuhan, China) for inflammatory cytokines: The Interleukin 6 (IL-6), Collagen Type I Alpha 1 (Col 1A1) concentrations in DMEM complete medium of HFFs and HSFs were tested using Human IL-6 ELISA Kit, human collagen I ELISA Kit, respectively, as being in line with the Sandwich-ELISA principle from the manufacturer. HFFs and HSFs with a density of 5×10^5 cells respectively were seeded on NY-exo and cultured for 24 h, then the supernatants were isolated at 1000 rpm for 5 min. Lipopolysaccharides (LPS, Sigma-Aldrich, USA) with a concentration of 1 $\mu\text{g}/\text{ml}$ as a positive control group for immune indicators were dissolved in culture medium with HFFs and HSFs respectively, and cells were cultured for 24 h. Cells without any NY-exo and LPS treatment served as control. The optical density (OD) was measured at 450 nm ($n = 5$).

Detection of Malondialdehyde (MDA) and Reactive Oxygen Species (ROS): To measure the lipid peroxidation in the supernatant, MDA was measured by using ELISA kits (Elabscience, Wuhan, China), according to the Competitive-ELISA principle from the manufacturer. Then, the OD value was measured using the same method as above ($n = 3$). HFFs and HSFs were seeded on NY-exo respectively as above statement. Hydrogen peroxide (H_2O_2) solution with a concentration of 20 μM was as a positive control group for MDA and ROS indicators and mixed with cells for 24 h. Cells without any NY-exo and H_2O_2 treatment served as control. The production of active oxygen in HFFs and HSFs was measured by the Reactive Oxygen Species Assay Kit (Beyotime, Nantong, China).

CCK-8: To evaluate the cell viability, HFFs and HSFs with a density of 1×10^5 cells respectively seeded on NY-exo were incubated at $37\text{ }^{\circ}\text{C}$ for 4 h to evaluate cell viability using Cell counting kit-8 (CCK-8, Beyotime, Nantong, China). 1% fetal bovine serum (FBS) mixed with cells for 24 h as a positive control group. Cells without any NY-exo and FBS treatment served as control. The OD was determined at 450 nm via a microplate reader ($n = 5$).

Molecular detection of DNA damage: HFFs with a density of 5×10^5 seeded on NY-exo was cultured 24 h- H_2O_2 solution with a concentration of 20 μM was as a positive control group for $\gamma\text{-H2AX}$ indicators and mixed with HFFs for 24 h. Cells without any NY-exo and H_2O_2 treatment served as control. The HFFs were stained by Recombinant Anti-Histone H2AX antibody (Abcam, UK) according to the manufacturers' instructions and observed with a confocal microscope ($n = 3$).

2.13. Rabbit urethroplasty

All the animal experiments were in accordance with the guidelines for animal care. The animal protocol (SYXK 2017-0240) was approved by the animal ethics committee of Shanghai Sixth People's Hospital, Shanghai, China. All the adult New Zealand white rabbits were with average body weight (BW) \sim of 3.5 kg and were provided by the Shanghai Academy of Agricultural Sciences.

Six adult male New Zealand white rabbits were randomly divided into 2 groups. These rabbits were firstly pretreated with Ketamine (15 mg/kg), then xylazine (3 mg/kg) and acepromazine (0.75 mg/kg), finally anesthetized and maintained with 2% isoflurane. In group 1, the urethras of 3 rabbits were repaired with a non-ADSC-exos nanoyarn scaffold. In group 2, the remaining urethras of 3 rabbits were repaired with ADSC-exos nanoyarn scaffold. Each rabbit was performed by general anesthesia with intravenous injection of pentobarbital. The skin was sectioned at approximately 3 cm proximal to the external urethral orifice, and the urethra lumen was exposed. Ventral urethral defects with a mean length \times width of 2.0 cm \times 0.8 cm were created in the anterior urethra of rabbits. The scaffolds with a length \times width of 2.0 cm \times 1.0 cm were sutured to the edge of the defect using 5-0 absorbable polyglactin sutures. After the sutures, an F6 catheter was left in the urethra and fixed to the gland with 5-0 absorbable sutures for 28 days postoperatively. The animals were observed twice a day. All the rabbits

were euthanized in the experiments after 28 days, and the urethral tissue for the following histology staining was collected.

2.14. Histology and Immunofluorescent analysis

The specimens were immediately fixed in 4% paraformaldehyde solution for 4 h at room temperature, after which the samples were dehydrated and cleared through graded alcohols, and finally embedded in the paraffin blocks. To evaluate the epithelium and collagen distribution of the urethral tissue, histological sections were prepared and stained with hematoxylin and eosin (H&E) and Masson staining. To further demonstrate the repair urethral function, the samples were stained for immunofluorescence for CD31 (1:100, Proteintech Group, Inc), CD206 (1:500, Proteintech Group, Inc), PCNA (Proliferating Cell Nuclear Antigen 1:500, Abcam plc), cytokeratin AE1/AE3 (Santa Cruz Biotechnology, Inc.), and COL I. Afterwards, the specimens were imaged and observed by optical microscope.

2.15. Statistical analysis

The results were expressed as mean \pm standard deviation. Differences between experimental groups were analyzed using the paired-samples *t*-test or one-way ANOVA. All the analyses were performed by GraphPad Prism8 Software. It was statistically significant based on $p < 0.05$.

3. Results and discussion

3.1. Multipotency assay of ADSCs and characterization of ADSC-exos

Fig. 1a shows that the morphology of ADSCs is typical, fibroblast-like, that is, shuttle-shaped, and ADSCs themselves have a short spindle or oval shape at 3 days, then gathered at the bottom of the culture flask and grew into a whirlpool shape after 4 days. After induction of adipogenic differentiation, the lipid vacuoles were presented in the cell cytoplasm. The differentiated cells stained with Oil red O were

aggregated to form lipids droplets (Fig. 1b). For osteogenic differentiation, the differentiated cells formed mineralized nodules after alizarin red S staining (Fig. 1c). The induction of chondrogenic differentiation was assessed using Alcian Blue staining, revealing that cartilage specific proteoglycans had formed in the cultures (Fig. 1d). The expression levels of VEGFA, TIMP2, and WNT1 are 0.69 ± 0.45 , 1.56 ± 0.71 , and 0.00094 ± 0.00059 , respectively (Fig. 1e). ADSCs can secrete VEGFA and promote the angiogenesis of endothelial cells. TIMP2 conducts the proteolytic activity of all matrix metalloproteinases (MMPs). And the balance is maintained between ECM breakdown and synthesis [33]. The expression level of WNT1 is extremely low, so the Wnt/b-catenin signaling cannot be activated. The Wnt1 protein is considered as the activation of Wnt/b-catenin signaling [34]. Fig. 1 f shows that the exosomes are round, membrane-bound vesicles, that is, have double-membraned structures. Fig. 1 g shows the particle diameter analysis. The size distribution of exosomes is centered at 80–130 nm. The size distribution based on dynamic light scattering is slight > 100 nm.

3.2. Morphology and characteristics of scaffolds

In the field of nanofibers preparation, electrospinning is an energy-saving, highly efficient and environmentally friendly technology and has a wide range of selected materials, high specific surface area and porous structure [35]. The schematic of co-axial electrospinning and conjugated electrospinning set-ups is shown in Fig. 2a and c, respectively. Compared with the chaotic arrangement of the nanofibers, the fibers in the nanoyarn were arranged neatly and toward the same direction. The SEM images of different scaffolds reveal that the angle distribution of ADSC-exos (50%) nanoyarn over non-ADSC-exos nanoyarn were not significantly different, as seen in Fig. 2b, d and e. The angle of the nanofibers in the ADSC-exos nanoyarn and non-ADSC-exos nanoyarn mainly ranges from $0^\circ \sim 20^\circ$, but the angle of the nanofiber scaffolds spreads between 0° and 100° . The core-shell structure of ADSC-exos nanoyarn and non-ADSC-exos nanoyarn were observed by Transmission Electron Microscopy (TEM), as seen in Fig. 2f and g. TEM

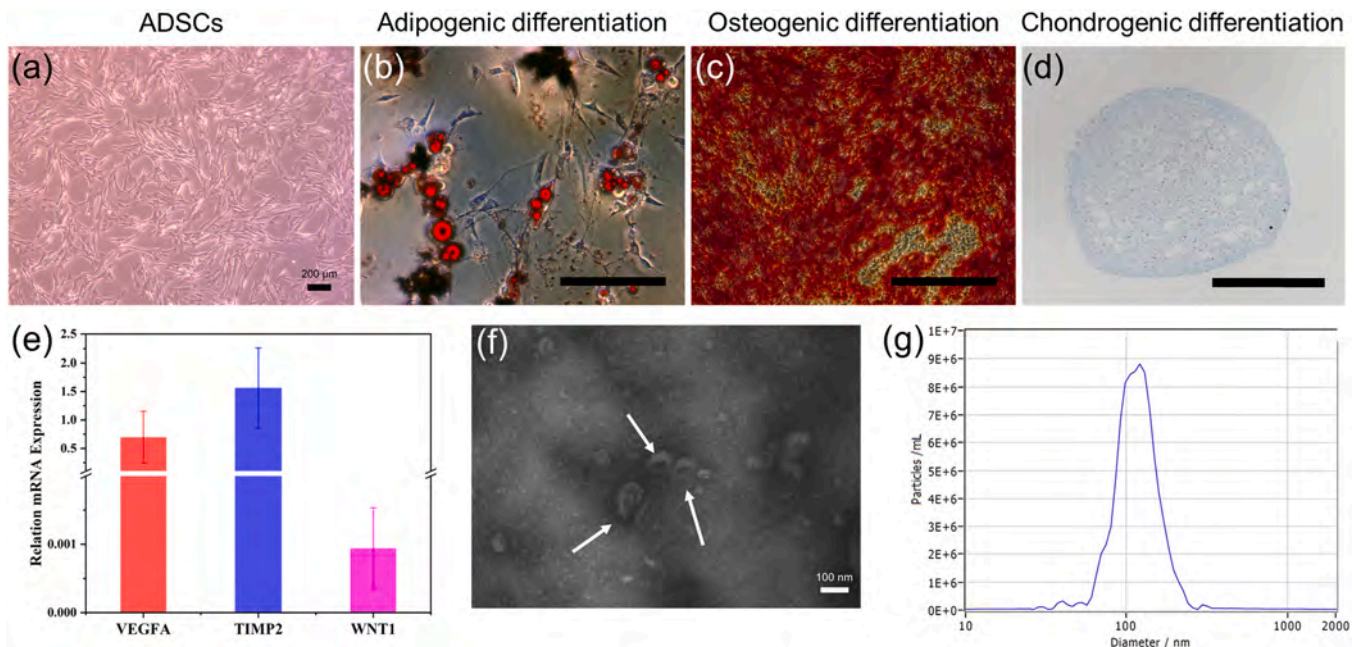


Fig. 1. Adipogenic, Osteogenic and chondrogenic differentiation of ADSCs and characterization of ADSC-exos. (a) Optical microscope of ADSCs morphology. (b) The Oil red O staining of the adipogenic differentiation. (c) The alizarin red S staining of the osteogenic differentiation. (d) The Alcian blue staining of chondrogenic differentiation (b-c: $\times 200$ magnification). (e) The paracrine activity of ADSCs and the expression of proteins (VEGFA: angiogenic factors related genes; TIMP2: trophic proteins; WNT1) by PCR analyses. (f) TEM image of ADSC-exos shows that the diameter is approximately 100 nm and they are pointed by the white arrows. (g) Size distribution of exosomes as measured by NTA.

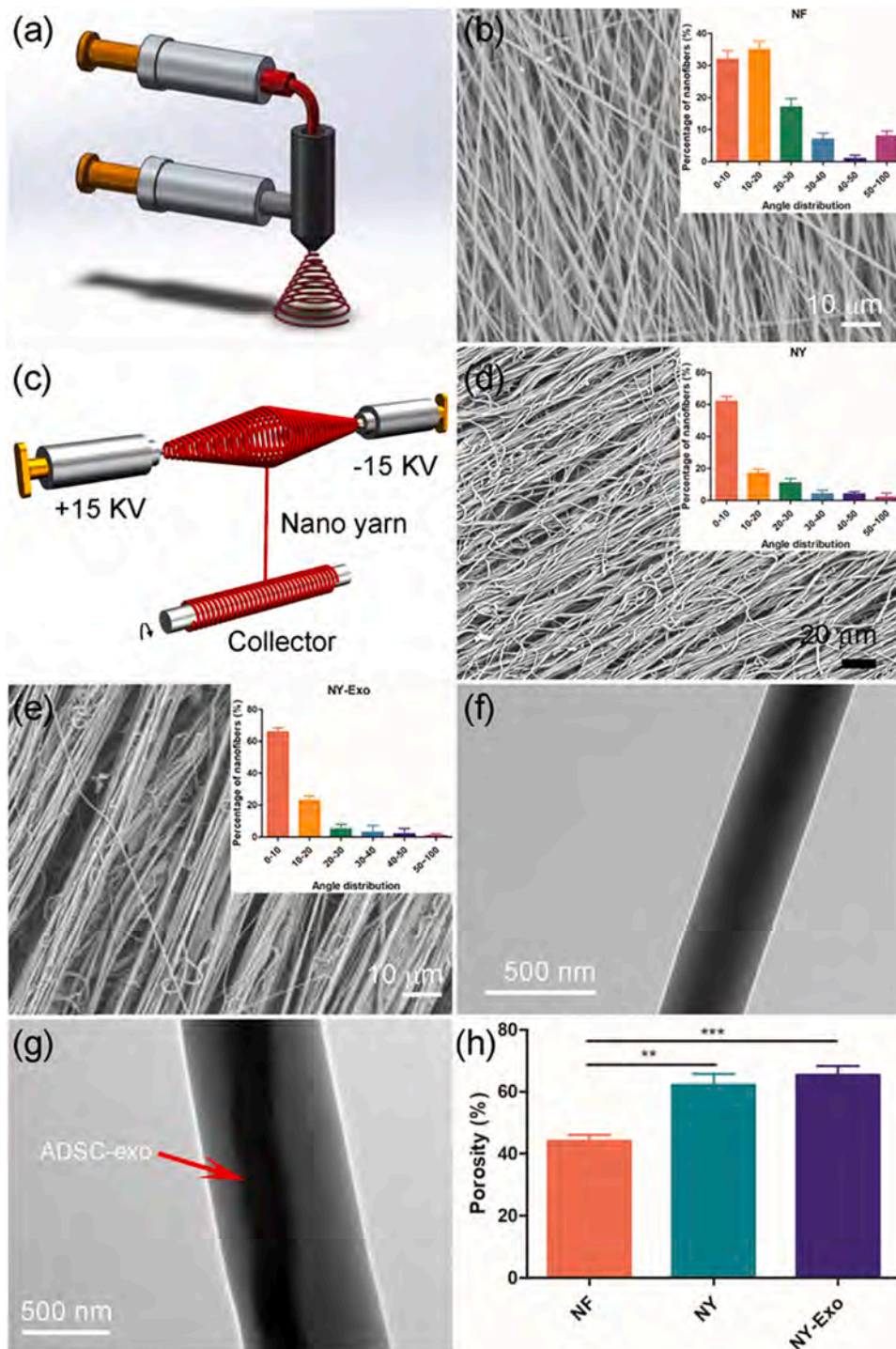


Fig. 2. Schematic of electrospinning and SEM and TEM images of the morphology of nanofibers, and their angular distributions of fibers ($n = 100$). (a) Schematic of co-axial electrospinning and (c) conjugated electrospinning; SEM images of (b) nanofiber scaffold, (d) non-ADSC-exos nanofiber scaffold and (e) ADSC-exos with a concentration of 50% nanofiber scaffold and their angular distributions of fibers; TEM images of (f) non-ADSC-exos nanofiber scaffold and (g) ADSC-exos nanofiber scaffold; (h) Porosity of different scaffolds. (** $P < 0.01$; *** $P < 0.001$).

images show that the core-shell structure included Col/P(LLA-CL) in the shell and ADSC-exos with a concentration of 50% in the core, and the fibers were uniform, cylindrical and the surfaces were smooth, as seen in Fig. 2g. The core/shell structure for the controllable drug delivery systems is a good candidate [10,36]. At present, the main methods of delivering exosomes on the scaffold are adhesion (physical adsorption) and encapsulation [37–39]. There have been some studies reporting that exosomes were seeded on the surface of nanofibers scaffold through adsorption and released continuously [39,40]. The exosomes are a specific class of lipid-membrane bound extra-cellular vesicles, and the exosomes contain organic compounds of cells, like mRNAs and proteins.

Additionally, nanofiber can adsorb organic compounds on its surface. So, the ADSC-exos may be combined through physical adsorption with Collagen and P (LLA-CL). Compared with the porosity in the nanofiber scaffold ($44.15 \pm 2.1\%$, mean \pm std), the nanofiber porosity ($62.28 \pm 3.4\%$, ** $P < 0.01$) and the ADSC-exos nanofiber porosity ($65.46 \pm 2.8\%$, *** $P < 0.001$) increased significantly, as seen in Fig. 2 h. Therefore, the porosity of nanofiber was larger than the nanofiber scaffold, which would efficiently allow material infiltration from tissues containing penetrating fluid.

3.3. Mechanical properties of electrospun scaffolds

The mechanical property of nanofiber scaffolds is an important factor in the practical application to urethral repair and tissue regeneration. The mechanical properties of the native rabbit urethra were presented in previous experiments [41]. To evaluate the mechanical characteristics of the nanoyarn with or without ADSC-exos for in vivo experiments, the mechanical properties of NY and NY-Exo (the concentration of ADSC-exos was 50%), are shown in Fig. 3a-d. NY is higher than NY-exo in tensile stress, Young's modulus, and tensile strength at break, but lower in strain at break. The ADSC-exos nanoyarn seems to reduce an elevation of Young's modulus (7.92 ± 0.02 MPa), as seen in Fig. 3b, and the tensile strength as seen in Fig. 3c. However, the elevation of strain at break in the ADSC-exos nanoyarn scaffold was not significant compared with nanoyarn scaffold (NY: $60.2 \pm 0.01\%$, NY-exo: $62.3 \pm 0.05\%$, respectively), as seen in Fig. 3d. On the whole, the tensile strength and elastic modulus of the nanoyarn scaffold were relatively large, and the yield point was centered at 60–70% strain. The properties of nanoyarn scaffolds with ADSC-exos are more suitable in the rabbit model operation.

3.4. Cell Proliferation on Scaffold

To evaluate the proliferation of human foreskin fibroblasts (HFFs), with different concentrations of ADSC-exos nanoyarn scaffolds, they were measured by the MTT assay at days 1, 3, 5. As seen in Fig. 4, the cell viability of HFFs was increased when cultured with ADSC-exos. Furthermore, with the increase of concentration of ADSC-exos, proliferation was also significant. By day 1, there is no significantly fluctuation in all Exo@Col/PLCL groups [0.3 ± 0.02 (25% Exo@Col/PLCL), 0.28 ± 0.02 (50% Exo@Col/PLCL), 0.28 ± 0.02 (75% Exo@Col/PLCL)]. All groups show high cell viability at day 5, with 50% ADSC-exos nanoyarn scaffold having the highest MTT (2.08 ± 0.03) ($*P < 0.05$). Notably, 75% Exo@Col/PLCL (0.9 ± 0.01 , 1.78 ± 0.03 , respectively) is significantly less MTT than 50% Exo@Col/PLCL at days 3 and 5 ($*P < 0.05$). The results show that ADSC-exos with a different concentration could promote the proliferation of fibroblasts; the porous structure of the nanoyarn scaffold was also a benefit to cell growth. Some studies had shown that exosomes function in cell proliferation played a direct role in a paracrine or endocrine manner [42–45]. Exosomes significantly increased cell proliferation in a dose-dependent manner [42].

3.5. Biocompatibility and cytotoxicity analysis

To explore the biocompatibility and cytotoxicity of ADSC-exos nanoyarn scaffold for cells, the verification of experiments was performed. We designed the cells without the nanoyarn scaffold group

(control group), the experiment group of ADSC-exos nanoyarn scaffold, and the positive control group respectively stimulated by LPS, H_2O_2 , and FBS. In addition, the degree of toxicity and inflammation of these groups in different cells were compared.

The inflammatory factor IL-6 level in NY-exo group [37.91 ± 8.58 (HFFs), 19.86 ± 5.46 (HSFs), respectively] was higher than that in the control group [12.95 ± 3.94 (HFFs), 16.18 ± 1.74 (HSFs), respectively] in the two different cells of HFFs and HSFs ($***P < 0.001$). Besides, the secretion of IL-6 in HSFs was significantly lower than that in HFFs, indicating that the degree of inflammation was reduced. The expression of IL-6 inside and outside the cells was promoted by the stimulation of Lipopolysaccharide (LPS) [149.04 ± 25.30 (HFFs), 103.97 ± 6.73 (HSFs), respectively] ($***P < 0.001$). This shows that LPS may cause HFFs and HSFs cell damage, and more serious for HFFs, as seen in Fig. 5a. Similarly, the deposition of collagen type I alpha 1 (Col 1A1) in cells appeared. In NY-exo group [18.91 ± 4.50 (HFFs), 21.01 ± 7.26 (HSFs), respectively], the amount of deposited Col 1A1 was higher than that in the control group [4.11 ± 1.24 (HFFs), 3.89 ± 2.02 (HSFs), respectively] ($***P < 0.001$), and the content of Col 1A1 in HSFs was slightly higher than that in HFFs, as seen in Fig. 5b. The deposition of considerable Col 1A1 was caused by the stimulation of LPS [61.63 ± 12.77 (HFFs), 52.23 ± 9.75 (HSFs), respectively] ($***P < 0.001$). The tissue tensile strength and the effect of wound healing were improved by proper collagen deposition [46,47]. However, the excessive deposition will lead to fibrosis because Col 1A1 is the main component of the extracellular matrix. Our results indicate that the degree of fibrosis HFFs was higher than that of HSFs.

Both cell lines were treated with NY-exo and FBS, and the cell viability was studied using CCK-8 assay. The results showed that the ADSC-exos nanoyarn scaffold significantly promoted cell proliferation and improved cell viability [1.15 ± 0.16 (HFFs), 1.03 ± 0.14 (HSFs), respectively], as compared with the control group ($**P < 0.01$). In contrast, the cell viability was greatly reduced upon being cultured with 1% FBS, which causes an inhibitory effect for cell growth [0.50 ± 0.16 (HFFs), 0.71 ± 0.07 (HSFs), respectively] ($***P < 0.001$), as seen in Fig. 5c.

To investigate the degree of cell oxidative damage, the levels of ROS and MDA of cells were seeded on the ADSC-exos nanoyarn scaffold and the cells were exposed to H_2O_2 as the positive control group was measured. ROS and MDA are the indicators for oxidative stress and the hallmark of lipid peroxidation, respectively. Compared with the control group, the production of the ROS in the supernatant of HFFs and HSFs seeded respectively on the NY-exo did not change much [0.93 ± 0.16 (HFFs), 0.96 ± 0.23 (HSFs), respectively]. Similarly, the production of the MDA on the NY-exo with cells was slightly change compared with the control group [NY-exo: 14.05 ± 3.59 (HFFs), 11.01 ± 0.85 (HSFs); CTRL: 14.84 ± 3.12 (HFFs), 9.88 ± 1.69 (HSFs), respectively]. However, our results show that H_2O_2 induced the upregulation of MDA and

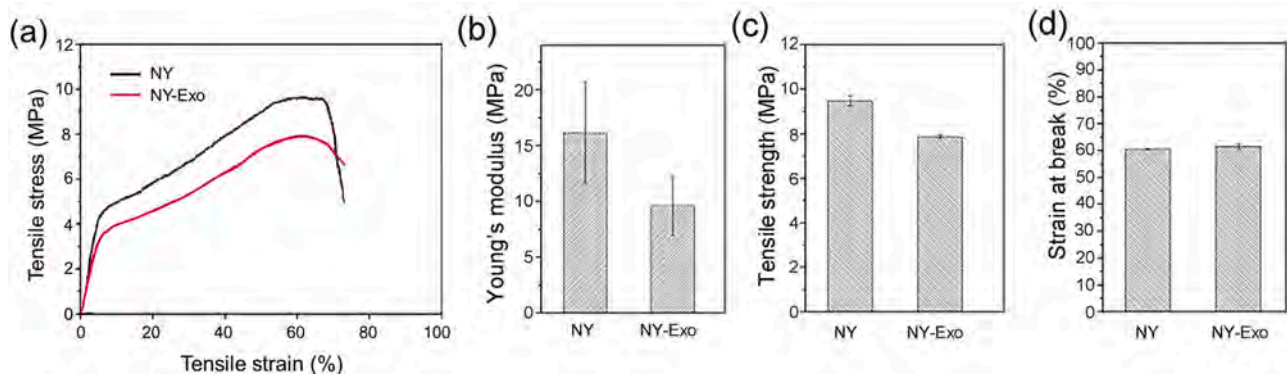


Fig. 3. Mechanical properties of nanoyarn scaffolds with or without ADSC-exos: (a) Tensile stress–strain curves; (b) Young's modulus; (c) Tensile strength at break; (d) strain at break.

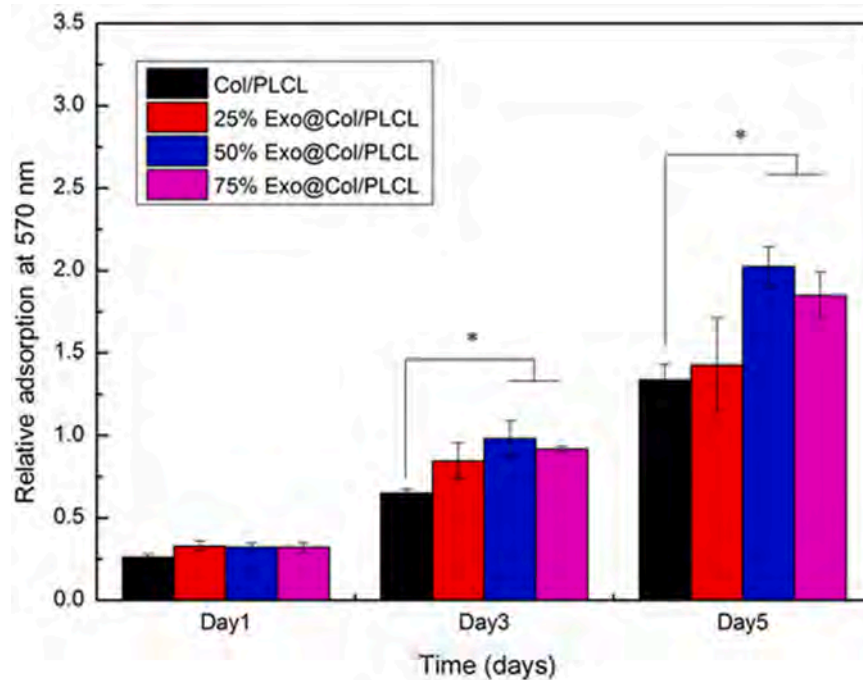


Fig. 4. Relative absorption of HFFs measured at the different concentrations of ADSC-exos nanoyarn scaffolds (0, 25%, 50%, 75%) for control on 1, 3, 5d by MTT assay. (* $P < 0.05$).

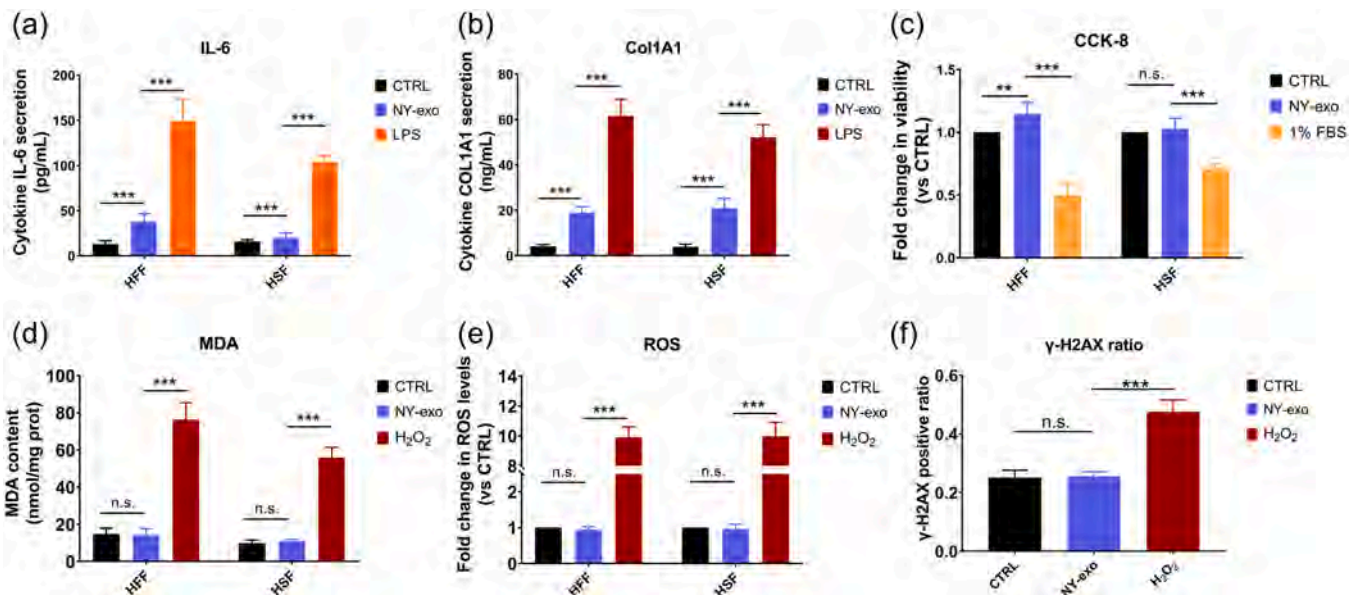


Fig. 5. Detection of biocompatibility and cytotoxicity of control group (cells only), experiment group (cells seeded on NY-exo), and positive control group (cells respectively stimulated by LPS, H₂O₂ and FBS). Measurement of inflammatory cytokines (a) IL-6 and (b) Col 1A1; (c) CCK-8; Cell oxidative damage (d) MDA and (e) ROS; (f) Molecular detection of DNA damage: γ -H2AX. (** $P < 0.01$; *** $P < 0.001$; n.s. means not significant).

ROS in HFFs and HSFs as seen in Fig. 5d and e [MDA: 76.32 ± 9.07 (HFFs), 55.85 ± 5.60 (HSFs); ROS: 9.92 ± 1.20 (HFFs), 9.99 ± 1.59 (HSFs), respectively] (** $P < 0.01$). Especially, the content of MDA increased obviously in HFFs. To evaluate the effects of NY-exo and H₂O₂ on DNA damage, γ -H2AX is considered to be one of the important markers of DNA damage [48]. As shown in Fig. 5f, the HFFs seeded on NY-exo did not contribute to DNA damage in the same way as did the normal cell's growth [NY-exo: 0.26 ± 0.02 ; CTRL: 0.25 ± 0.03 , respectively]. DNA damage to cells was more serious by H₂O₂ (0.48 ± 0.04) (** $P < 0.01$).

Overall, these results indicate that the safety of the NY-exo could be guaranteed. Although the nanoyarn biomaterials induced a certain degree of toxicity and inflammation, it was far lower than the positive control group.

3.6. FITC-labeled phalloidin staining

The human foreskin fibroblasts (HFFs) on the nanoyarn scaffolds were stained with FITC-labeled phalloidin and DAPI and were detected by immunofluorescence. The results for actin staining were shown in

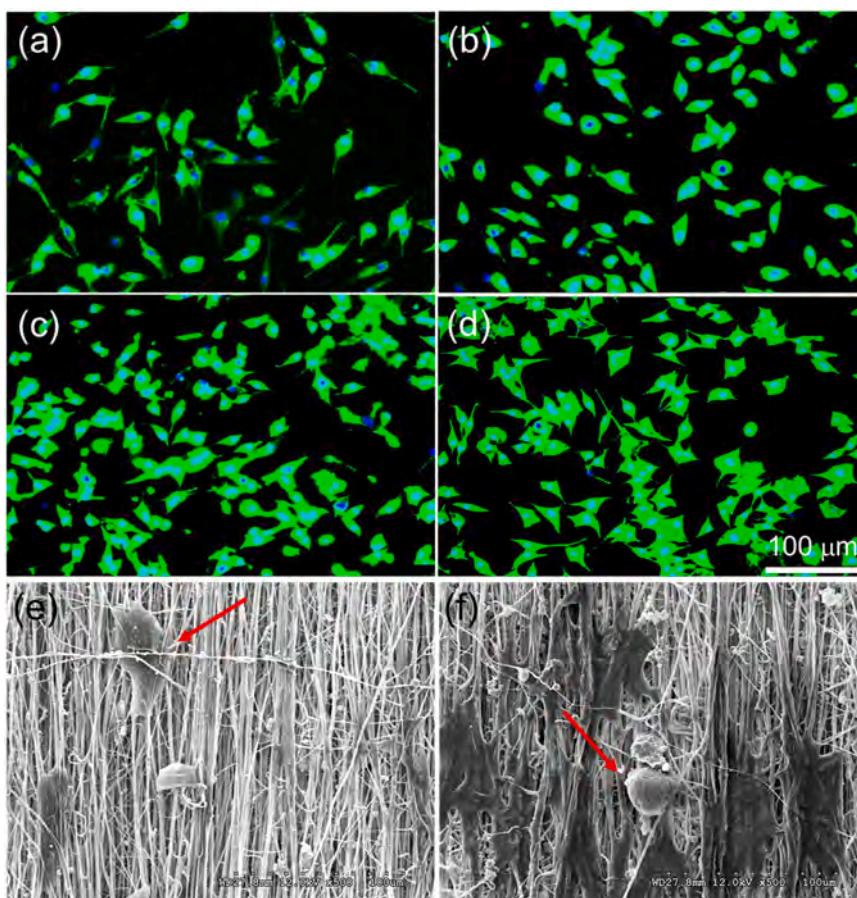


Fig. 6. Confocal microscopy and SEM image of human foreskin fibroblasts (HFFs) on different nanoyarn scaffolds. HFFs on non-ADSC-exo nanoyarn scaffold at day 3 (a) and day 5 (b), and ADSC-exo nanoyarn scaffold at day 3 (c) and day 5 (d). Scale bar: 100 μm . SEM image showed that HFFs expanded on non-ADSC-exo nanoyarn scaffold (e) and ADSCs-exo nanoyarn scaffold (f) at day 3 (Red arrows indicate HFFs). Scale bar:100 μm .

Fig. 6. The growth of the fibroblasts on the non-ADSC-exo nanoyarn scaffold did not show the typical morphology of extending outwards at day 3 in Fig. 6a and day 5 in Fig. 6b. Interestingly, when HFFs were seeded on the ADSC-exo nanoyarn scaffold, plenty of cells showing typical morphology of extending outwards were observed. This may indicate that fibroblasts promoted good growth and proliferation on ADSC-exo nanoyarn scaffold. The fibroblasts spreading on the scaffold were observed at day 3 in Fig. 6c and day 5 in Fig. 6d, and the morphology of cells obviously grew and the distribution of cells was spread evenly.

Cultured human foreskin fibroblasts with a density of 5×10^6 cells/ cm^2 were seeded onto each scaffold. To verify the physical properties of biomaterials for HFFs cell growth, the cell morphology of nanoyarn scaffolds with or without ADSC-exos was observed under SEM. SEM showed that the HFFs were attached on nanoyarn scaffolds at days three (Fig. 6e and f). The cells' growth was along the direction of yarns and stretched peripherally, however, the cells laden on the nanoyarn were relatively less, which was indicated that cells might not adhere to the nanoyarn biomaterials easily.

3.7. Urethroplasty examinations and histological analysis

To further evaluate the safety and influence of nanoyarn scaffolds with or without ADSC-exos, the histology analysis of urethral tissue reconstruction was performed. In the previous experiments, the urethroscopy and urethrography examinations for urethras have proved the NY was degradable, and the histological examination of urethras repaired with nanoyarn shows the NY was in good biocompatibility [1]. Granulation tissues were examined by H&E stained sections, and

collagen deposition and tissue fibrosis were assessed through Masson Trichrome staining. After the defects were introduced into the normal rabbit urethral model, urethroplasty was performed by implanting both the non ADSC-exo nanoyarn scaffold in Fig. 7a, and the ADSC-exo nanoyarn scaffold in Fig. 7e, into the defect model with running sutures. The nanoyarn with or without ADSC-exos was convenient to operate and suture, and the urethral was checked for recovery condition after 4 weeks post-surgery.

In the control group, it was suggested that fibrosis was associated with scar formation because the urothelium looked pale, and the hyperplasia of the scar was pointed by the blue arrow, as seen in Fig. 7b. Besides, a discontinuous epithelial layer was formed on the urethra lumen surface, and the urethral epithelium in the lumen was very thin (Fig. 7c). There was a large amount of collagen with a disorderly arrangement and less smooth muscle in the urethra lumen according to the Masson staining, as seen in Fig. 7d. Due to the failure of regenerated urethral SMCs to timely fill the degraded PLLA scaffold, the contractility of the regenerated urethral smooth muscle tissue was insufficient, resulting in urethral stricture. In contrast, in the urethras repaired with the ADSC-exo nanoyarn scaffold after 4 weeks post-surgery, urethral stricture or scar formation was not found as seen in Fig. 7f. In the histology test of the experiment group, a continued and complete epithelial layer was formed on the lumen surface and the epithelial cells formed multiple layer epithelium according to the H&E staining, as seen in Fig. 7g. Importantly, the appearance of the urethral defect and histological examination did not show a strong inflammatory response, indicating that the nanoyarn with good biocompatibility.

The submucosal tissue was developed into smooth muscle tissue (red) layers and the collagen layers (blue) were arranged regularly and

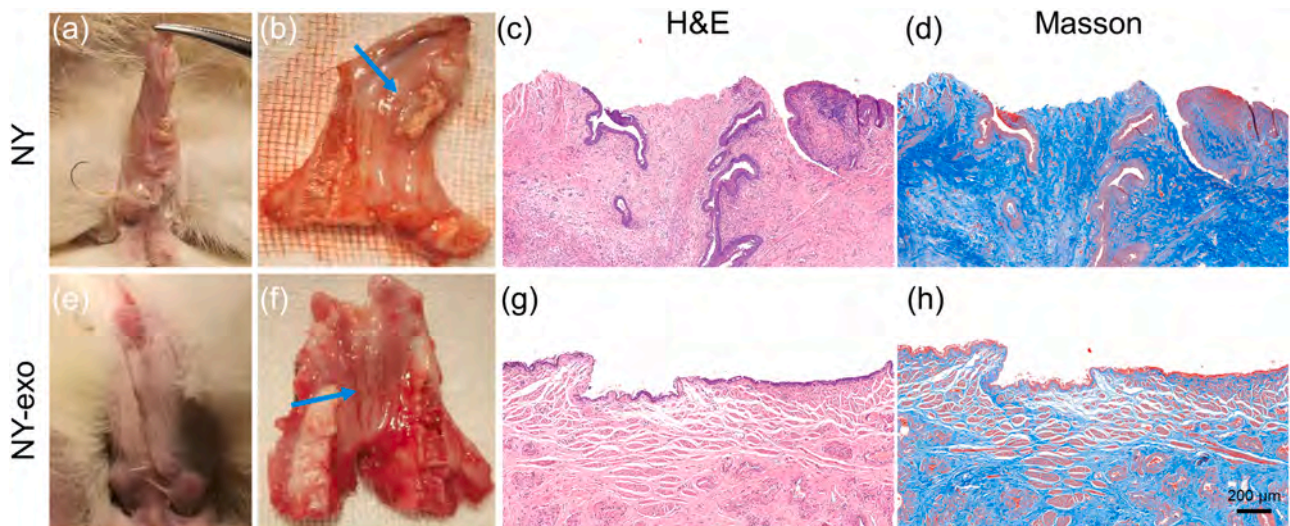


Fig. 7. Appearance of urethral defect model and urethral repair with biomaterial after 4 weeks post-surgery, and histological examination. (a-d) the control group and (e-h) the experiment group. Appearance of rabbit urethra model: (a, b, e, f). Urethras repaired were analyzed based on H&E (c, g); Manson (d, h).

relatively sparse in the Masson staining image, as seen in Fig. 7h. Our results show that the ADSC-exos nanoyarn scaffold has a good potential for the treatment of urethral defects in clinical application.

3.8. Immunofluorescence

Immunofluorescence staining of the regenerated section in urethral repair was employed to determine the expression of AE1/AE3 (epithelial cyokeratin, an important membrane surface protein marker of ECs) to study the distribution of cyokeratin (Fig. 8a). The expression level for AE1/AE3 on the ADSC-exos nanoyarn is significantly higher than this on the nanoyarn (Fig. 8c, **p < 0.01). Moreover, the nanoyarn results in a repair with the epithelial layer that could not get a complete regeneration. There was little or trace expression of cyokeratin. The process of angiogenesis includes the proliferation and migration of endothelial cells and the formation of the tube [49,50]. We sought to verify whether the ADSC-exos nanoyarn neovascularization observed in vivo was

associated with ADSC-exos. ADSC-exos nanoyarn-treated group showed more blood vessels than the nanoyarn group, as shown in Fig. 8b and f. It was demonstrated that ADSC-exos have the potential to promote angiogenesis.

To determine ADSC-exos for effective inhibition of fibrotic factors expression, the content of Collagen I was measured. The distribution of Collagen I on the nanoyarn group was disorder, as shown in Fig. 8d and h. In contrast, there was little expression of Collagen I for the ADSC-exos nanoyarn group, consisting of the results of Masson staining. The results showed that ADSC-exos inhibit the over-expression of Collagen I. There are different degrees of inflammation to the injured site due to the transplantation of external scaffolds in vivo. Thus, immunofluorescence-labeled staining was performed on the macrophages surrounding the nanoyarn and ADSC-exos nanoyarn (Fig. 8e). The results showed that the number of CD206 positive cells in the ADSC-exos nanoyarn-treated group was higher than the nanoyarn group, indicating the low level of local inflammatory response was caused by ADSC-exos treated group.

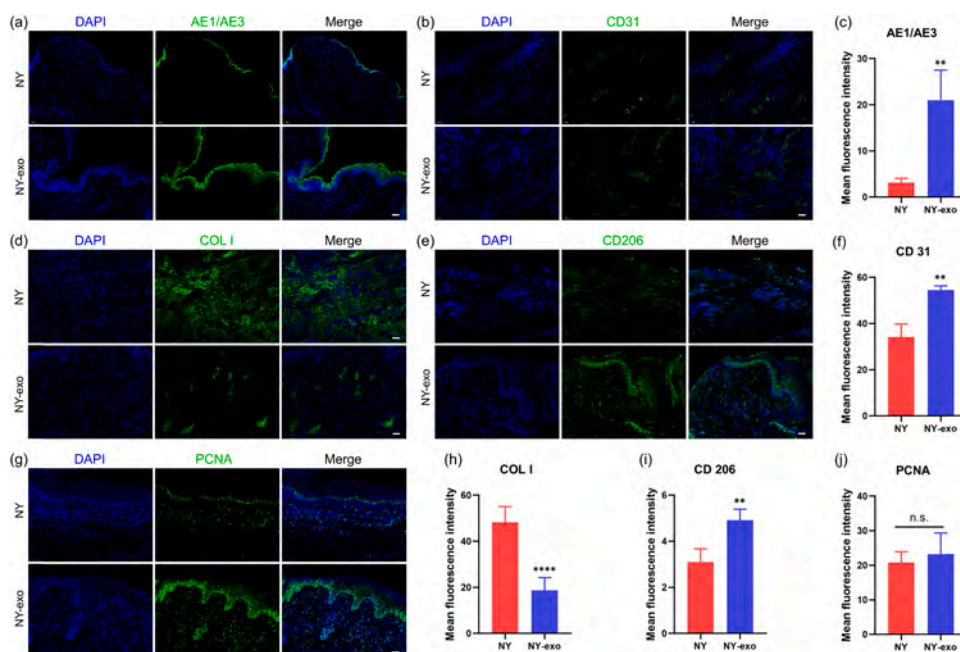


Fig. 8. Immunofluorescence staining of specific biomarkers in the NY and NY-exo repair after 4 weeks post-surgery. Representative immunofluorescence images of AE1/AE3 (a), CD31(b), COL I (d), CD206 (e), (g) PCNA. Scale bar: 50 μm. Blue: Nuclei. Quantification of expression levels of epithelial cyokeratin AE1/AE3 (c), the blood vessels based on the CD 31 (f), collagen type 1(h), the inflammation based on CD206 (M2 macrophages) (i), and cell proliferation based on PCNA (j). Data are means ± standard error, n = 3. **p < 0.01, ****p < 0.0001, n.s. means not significant.

But nanoyarn group caused extensive inflammatory response Fig. 8i. It was indicated that ADSC-exos appear to promote the transition of M2 macrophages and inhibit the inflammatory response during the urethral repair. In addition, due to inflammatory response in the ADSC-exos treated group was lower than the nanoyarn group, the positive expression of proliferating cell nuclear antigen (PCNA) was slightly increased (Fig. 8g and j). After urethral mucosa injury, fibroblasts were activated and proliferated. The formation of epithelial tissue facilitated the urethral repair due to the migration of fibroblasts. Our results revealed that ADSC-exos effectively promote epithelization, neovascularization, attenuated inflammation. The ADSC-exos-treated group did not promote the over-proliferation of fibroblasts and the expression of Collagen I.

4. Conclusion

In this study, we demonstrate that the ADSC-exos collagen/P(LLA-CL) nanoyarn scaffold has sufficient biocompatibility and mechanical properties, and can promote cell proliferation and tissue regeneration. The differentiation of adipogenic, osteogenic, and chondrogenic confirms the multipotential differentiation potential of ADSCs. ADSC-exos effectively promote neovascularization and attenuated inflammation. The urethra repair of ADSC-exos nanoyarn scaffold did not result in urethral stricture or scar formation, the less deposition of collagen, and the formed multiple-layer epithelium. Besides, ADSC-exos were easily obtained and could promote wound healing of urethra tissue, so to be an advanced therapeutic tool in research and clinical treatment. To some extent, the scaffold mimicked the native tissue matrix morphology and structure and may be applied to urethroplasty. We believe ADSC-exos nanoyarn scaffold may eventually serve as effective clinical implantation to repair urethral defects.

CRedit authorship contribution statement

Liyang Wang: Formal analysis, Investigation, Methodology, Writing – original draft. **Wei Cheng:** Formal analysis, Methodology. **Jingjing Zhu:** Investigation, Methodology. **Danyang Li:** Investigation. **Qiang Fu:** Resources, Supervision, Funding acquisition. **Xiumei Mo:** Resources, Supervision. **Xi Yang:** Conceptualization. **Weixin Zhao:** Resources, Supervision. **Mingjun Ren:** Validation, Visualization. **Jieji Ren:** Validation, Visualization. **Wenyao Li:** Writing – review & editing. **Kaile Zhang:** Funding acquisition, Conceptualization, Supervision, Writing – review & editing.

Declaration of Competing Interest

The authors declare that they have no known competing financial interests or personal relationships that could have appeared to influence the work reported in this paper.

Acknowledgements

This work was supported by the National Natural Science Fund of China (grant no. 81700590); the Shanghai Jiao Tong University Biomedical Engineering Cross Research Foundation (grant no. YG2017QN15, YG2021QN03); Shanghai Municipal Commission of Health and Family Planning (grant no. 20184Y0053); Shanghai Health Committee (20184Y0053); Shanghai "Rising stars of medical talent" Youth development program; Shanghai Jiao Tong University K. C. Wong Medical Fellowship Fund; Shanghai sixth people's hospital fundamental research fund. The Talent Program of Shanghai University of Engineering Science (QNTD202104), Shanghai Local Universities Capacity Building Project of Science and Technology Innovation Action Program (21010501700).

References

- [1] K. Zhang, X. Fang, J. Zhu, R. Yang, Y. Wang, W. Zhao, X. Mo, Q. Fu, Effective reconstruction of functional urethra promoted With ICG-001 delivery using core-shell collagen/poly (Lactide-co-caprolactone) [P(LLA-CL)] nanoyarn-based scaffold: a study in dog model, *Front. Bioeng. Biotechnol.* 8 (2020) 774.
- [2] A. Atala, M. Danilevskiy, A. Lyundup, P. Glybochko, D. Butnaru, A. Vinarov, J. J. Yoo, The potential role of tissue-engineered urethral substitution: clinical and preclinical studies, *J. Tissue Eng. Regen. Med.* 11 (1) (2015) 3–19.
- [3] T.O. Abbas, E. Mahdi, C.P. Pennisi, Current status of tissue engineering in the management of severe hypospadias, *Front. Pediatrics* 5 (2018) 283.
- [4] J. Leor, Y. Amsalem, S. Cohen, Cells, scaffolds, and molecules for myocardial tissue engineering, *Pharmacol. Therap.* 105 (2) (2005) 151–163.
- [5] D.E.P. Muylaert, J.O. Fledderus, C.V.C. Bouten, P.Y.W. Dankers, M.C. Verhaar, Combining tissue repair and tissue engineering; bioactivating implantable cell-free vascular scaffolds, *Heart* 100 (23) (2014) 1825–1830.
- [6] C. Pu, C. Liu, C. Liang, Y. Yen, S. Chen, Y.J. Shieh, C. Chien, Y. Chen, Y. Chen, Adipose-derived stem cells protect skin flaps against ischemia/reperfusion injury via IL-6 expression, *J. Investig. Dermatol.* 137 (6) (2017) 1353–1362.
- [7] C. Chapple, Tissue engineering of the urethra: where are we in 2019? *World J. Urol.* 38 (9) (2020) 2101–2105.
- [8] T.O. Abbas, H.C. Yalcin, C.P. Pennisi, From acellular matrices to smart polymers: degradable scaffolds that are transforming the shape of urethral tissue engineering, *Int. J. Mol. Sci.* 20 (7) (2019) 1763.
- [9] J. Kaewsaeene, F. Duriyart, V. Pavarajarn, Fabrication of flexible titania/polyacrylonitrile co-axial nanofibers via electrospinning, *J. Asian Ceramic Soc.* 8 (1) (2020) 203–210.
- [10] A. Joshi, Z. Xu, Y. Ikegami, S. Yamane, M. Tsurashima, H. Iijima, Co-culture of mesenchymal stem cells and human umbilical vein endothelial cells on heparinized polycaprolactone/gelatin co-spon nanofibers for improved endothelium remodeling, *Int. J. Biol. Macromol.* 151 (2020) 186–192.
- [11] S.H. Kim, S.K. Im, S.J. Oh, S. Jeong, E.S. Yoon, C.J. Lee, N. Choi, E.M. Hur, Anisotropically organized three-dimensional culture platform for reconstruction of a hippocampal neural network, *Nat. Commun.* 8 (1) (2017) 14346.
- [12] W.T. Tung, J. Zou, X. Sun, W. Wang, O.E.C. Gould, K. Kratz, N. Ma, A. Lendlein, P. Wiggemann, A. Krüger-Genge, F. Jung, Coaxial electrospinning of PEEU/gelatin to fiber meshes with enhanced mesenchymal stem cell attachment and proliferation, *Clin. Hemorheol. Microcirc.* 74 (1) (2020) 53–66.
- [13] K. Zhang, N. Cao, X. Guo, Q. Zou, S. Zhou, R. Yang, W. Zhao, X. Mo, W. Liu, Q. Fu, The fabrication of 3D surface scaffold of collagen/poly (L-lactide-co-caprolactone) with dynamic liquid system and its application in urinary incontinence treatment as a tissue engineered sub-urethral sling: In vitro and in vivo study, *NeuroUrol. Urodyn.* 37 (3) (2017) 978–985.
- [14] X. Guo, K. Zhang, M. El-Aassar, N. Wang, H. El-Hamshary, M. El-Newehy, Q. Fu, X. Mo, The comparison of the Wnt signaling pathway inhibitor delivered electrospun nanoyarn fabricated with two methods for the application of urethroplasty, *Front. Mater. Sci.* 10 (4) (2016) 346–357.
- [15] K. Zhang, X. Guo, Y. Li, Q. Fu, X. Mo, K. Nelson, W. Zhao, Electrospun nanoyarn seeded with myoblasts induced from placental stem cells for the application of stress urinary incontinence sling: An in vitro study, *Colloids Surf. B Biointerfaces* 144 (2016) 21–32.
- [16] Y. Bai, Y. Han, X. Yan, J. Ren, Q. Zeng, X. Li, X. Pei, Y. Han, Adipose mesenchymal stem cell-derived exosomes stimulated by hydrogen peroxide enhanced skin flap recovery in ischemia-reperfusion injury, *Biochem. Biophys. Res. Commun.* 500 (2) (2018) 310–317.
- [17] X. Li, X. Xie, W. Lian, R. Shi, S. Han, H. Zhang, L. Lu, M. Li, Exosomes from adipose-derived stem cells overexpressing Nrf2 accelerate cutaneous wound healing by promoting vascularization in a diabetic foot ulcer rat model, *Exp. Mol. Med.* 50 (4) (2018) 1–14.
- [18] X. Liang, Y. Ding, Y. Zhang, H.F. Tse, Q. Lian, Paracrine mechanisms of mesenchymal stem cell-based therapy: current status and perspectives, *Cell Transplant.* 23 (9) (2014) 1045–1059.
- [19] M. Song, J. Heo, J.Y. Chun, H.S. Bae, J.W. Kang, H. Kang, Y.M. Cho, S.W. Kim, D.-M. Shin, M.-S. Choo, The paracrine effects of mesenchymal stem cells stimulate the regeneration capacity of endogenous stem cells in the repair of a bladder-outlet-obstruction-induced overactive bladder, *Stem Cells Dev.* 23 (6) (2014) 654–663.
- [20] M. Kucharzewski, E. Rojczyk, K. Wilemska-Kucharzewska, R. Wilk, J. Hudecki, M. J. Los, Novel trends in application of stem cells in skin wound healing, *Eur. J. Pharm.* 843 (2019) 307–315.
- [21] L. Hu, J. Wang, X. Zhou, Z. Xiong, J. Zhao, R. Yu, F. Huang, H. Zhang, L. Chen, Exosomes derived from human adipose mesenchymal stem cells accelerates cutaneous wound healing via optimizing the characteristics of fibroblasts, *Sci. Rep.* 6 (1) (2016) 32993.
- [22] Y. Han, L. Jia, Y. Zheng, W. Li, Salivary exosomes: emerging roles in systemic disease, *Int. J. Biol. Sci.* 14 (6) (2018) 633–643.
- [23] H. Jing, X. He, J. Zheng, Exosomes and regenerative medicine: state of the art and perspectives, *Transl. Res.* 196 (2018) 1–16.
- [24] S. Jiang, G. Tian, Z. Yang, X. Gao, F. Wang, J. Li, Z. Tian, B. Huang, F. Wei, X. Sang, L. Shao, J. Zhou, Z. Wang, S. Liu, X. Sui, Q. Guo, W. Guo, X. Li, Enhancement of acellular cartilage matrix scaffold by Wharton's jelly mesenchymal stem cell-derived exosomes to promote osteochondral regeneration, *Bioact. Mater.* 6 (9) (2021) 2711–2728.
- [25] H. Valadi, K. Ekström, A. Bossios, M. Sjöstrand, J.J. Lee, J.O. Lötvall, Exosome-mediated transfer of mRNAs and microRNAs is a novel mechanism of genetic exchange between cells, *Nat. Cell Biol.* 9 (6) (2007) 654–659.
- [26] D.M. Pegtel, S.J. Gould, Exosomes, *Annu. Rev. Biochem.* 88 (2019) 487–514.

- [27] S. Buratta, B. Tancini, K. Sagini, F. Delo, E. Chiaradia, L. Urbanelli, C. Emiliani, Lysosomal exocytosis, exosome release and secretory autophagy: the autophagic- and endo-lysosomal systems go extracellular, *Int. J. Mol. Sci.* 21 (7) (2020) 2576.
- [28] S.R. Baglio, D.M. Pegtel, N. Baldini, Mesenchymal stem cell secreted vesicles provide novel opportunities in (stem) cell-free therapy, *Front. Phys.* 3 (2012) 359.
- [29] X. Liu, S. Wang, S. Wu, Q. Hao, Y. Li, Z. Guo, W. Wang, Exosomes secreted by adipose-derived mesenchymal stem cells regulate type I collagen metabolism in fibroblasts from women with stress urinary incontinence, *Stem Cell Res. Ther.* 9 (1) (2018) 159.
- [30] C.E. Ambrósio, M. García-Contreras, C.D. Vera-Donoso, J.M. Hernández-Andreu, J. M. García-Verdugo, E. Oltra, Therapeutic potential of human adipose-derived stem cells (adscs) from cancer patients: a pilot study, *PLoS ONE* 9 (11) (2014).
- [31] H.L. Wong, W.S. Siu, C.H. Fung, C. Zhang, W.T. Shum, X.L. Zhou, C.B.S. Lau, J. F. Zhang, P.C. Leung, W.M. Fu, C.H. Ko, Characteristics of stem cells derived from rat fascia: In vitro proliferative and multilineage potential assessment, *Mol. Med. Rep.* 11 (3) (2015) 1982–1990.
- [32] H. Zhang, N. Yu, Y. Zhou, H. Ma, J. Wang, X. Ma, J. Liu, J. Huang, Y. An, Construction and characterization of osteogenic and vascular endothelial cell sheets from rat adipose-derived mesenchymal stem cells, *Tissue Cell* 48 (5) (2016) 488–495.
- [33] M. Chen, M. Zhou, Y. Fu, J. Li, Z. Wang, Effects of miR-672 on the angiogenesis of adipose-derived mesenchymal stem cells during bone regeneration, *Stem Cell Res. Ther.* 12 (1) (2021) 85.
- [34] S. Luo, Q. Shi, Z. Zha, P. Yao, H. Lin, N. Liu, H. Wu, S. Sun, Inactivation of Wnt/β-catenin signaling in human adipose-derived stem cells is necessary for chondrogenic differentiation and maintenance, *Biomed. Pharmacother.* 67 (8) (2013) 819–824.
- [35] B. Komur, F. Bayrak, N. Ekren, M.S. Eroglu, F.N. Oktar, Z.A. Sinirlioglu, S. Yucel, O. Guler, O. Gunduz, Starch/PCL composite nanofibers by co-axial electrospinning technique for biomedical applications, *Biomed. Eng. Online* 16 (1) (2017) 1–13.
- [36] N. Rahimi Tanha, M. Nouri, An experimental study on the coaxial electrospinning of silk fibroin/poly (vinyl alcohol)–salicylic acid core-shell nanofibers and process optimization using response surface methodology, *J. Ind. Text.* 48 (5) (2017) 884–903.
- [37] L. Xina, X. Lina, F. Zhou, C. Li, X. Wang, H. Yu, Y. Pan, H. Fei, L. Ma, S. Zhang, A scaffold laden with mesenchymal stem cell-derived exosomes for promoting endometrium regeneration and fertility restoration through macrophage immunomodulation, *Acta Biomater.* 113 (2020) 252–266.
- [38] Y. Zhang, P. Zhang, X. Gao, L. Chang, Z. Chen, X. Mei, Preparation of exosomes encapsulated nanohydrogel for accelerating wound healing of diabetic rats by promoting angiogenesis, *Mater. Sci. Eng. C* (120) (2020), 111671.
- [39] M.G. Gandolfi, C. Gardin, F. Zamparini, L. Ferroni, M.D. Esposti, G. Parchi, B. Ercan, L. Manzoli, F. Fava, P. Fabbri, C. Prati, B. Zavan, Mineral-doped poly(L-lactide) acid scaffolds enriched with exosomes improve osteogenic commitment of human adipose-derived mesenchymal stem cells, *Nanomaterials* ((Basel)) 10 (3) (2020) 432.
- [40] F. Barati, A.M. Farsani, M. Mahmoudifard, A promising approach toward efficient isolation of the exosomes by core-shell PCL-gelatin electrospun nanofibers, *Bioprocess Biosyst. Eng.* 43 (2020) 1961–1971.
- [41] K. Zhang, Q. Fu, J. Yoo, X. Chen, P. Chandra, X. Mo, L. Song, A. Atala, W. Zhao, 3D bioprinting of urethra with PCL/PLCL blend and dual autologous cells in fibrin hydrogel: An in vitro evaluation of biomimetic mechanical property and cell growth environment, *Acta Biomater.* (2017) 154–164.
- [42] J. Ni, H. Li, Y. Zhou, B. Gu, Y. Xu, Q. Fu, X. Peng, N. Cao, Q. Fu, M. Jin, G. Sun, J. Wang, Y. Jin, F. Liu, Therapeutic potential of human adipose-derived stem cell exosomes in stress urinary incontinence – an in vitro and in vivo study, *Cell. Phys. Biochem.* 48 (4) (2018) 1710–1722.
- [43] H. Zhao, Q. Shang, Z. Pan, Y. Bai, Z. Li, H. Zhang, Q. Zhang, C. Guo, L. Zhang, Q. Wang, Exosomes from adipose-derived stem cells attenuate adipose inflammation and obesity through polarizing M2 macrophages and being in white adipose tissue, *Diabetes* 67 (2) (2018) 235–247.
- [44] B. Li, J. Yang, R. Wang, J. Li, X. Li, X. Zhou, S. Qiu, R. Weng, Z. Wu, C. Tang, P. Li, Delivery of vascular endothelial growth factor (VEGFC) via engineered exosomes improves lymphedema, *Ann. Transl. Med.* 8 (22) (2020) 1498.
- [45] J. Zhang, Y. Yi, S. Yang, Y. Zhu, X. Hu, Effects of adipose-derived stem cell released exosomes on proliferation, migration, and tube-like differentiation of human umbilical vein endothelial cells, *Zhongguo Xiu Fu Chong Jian Wai Ke Za Zhi* 32 (10) (2018) 1351–1357.
- [46] J. Wu, J. Zhu, C. He, Z. Xiao, J. Ye, Y. Li, A. Chen, H. Zhang, X. Li, L. Lin, Y. Zhao, J. Zheng, J. Xiao, Comparative study of heparin-poloxamer hydrogel modified bFGF and aFGF for in vivo wound healing efficiency, *ACS Appl. Mater. Interfaces* 8 (29) (2016) 18710–18721.
- [47] W. Gao, W. Jin, Y. Li, L. Wan, C. Wang, C. Lin, X. Chen, B. Lei, C. Mao, A highly bioactive bone extracellular matrix-biomimetic nanofibrous system with rapid angiogenesis promotes diabetic wound healing, *J. Mater. Chem. B* 5 (35) (2017) 7285–7296.
- [48] L. Zhao, D.W. Chang, Y. Gong, C. Eng, X. Wu, Measurement of DNA damage in peripheral blood by the γ-H2AX assay as predictor of colorectal cancer risk, *DNA Repair* 53 (2017) 24–30.
- [49] Y. Du, J. Ge, Y. Li, P.X. Ma, B. Lei, Biomimetic elastomeric, conductive and biodegradable polycitrate-based nanocomposites for guiding myogenic differentiation and skeletal muscle regeneration, *Biomaterials* 157 (2018) 40–50.
- [50] Y. Han, Y. Bai, X. Yan, J. Ren, Q. Zeng, X. Li, X. Pei, Y. Han, Co-transplantation of exosomes derived from hypoxia-preconditioned adipose mesenchymal stem cells promotes neovascularization and graft survival in fat grafting, *Biochem. Biophys. Res. Commun.* 497 (1) (2018) 305–312.